JVR
Journal of
Vascular Research

Research Article

J Vasc Res
DOI: 10.1159/000542481

Received: May 28, 2024
Accepted: November 3, 2024
Published online: January 17, 2025

Fibrillin-1 Deficiency Perturbs Aortic Cholinergic Relaxation and Adrenergic Contraction in a Mouse Model of Early Onset Progressively Severe Marfan Syndrome

Anna Cantalupo[a, b] Keiichi Asano[a] Sergey Dikalov[c] Dylan Gordon[a]
Francesco Ramirez[a]

[a]Department of Pharmacological Sciences, Icahn School of Medicine at Mount Sinai, New York, NY, USA; [b]Department of Pediatrics, Icahn School of Medicine at Mount Sinai, New York, NY, USA; [c]Division of Clinical Pharmacology, Vanderbilt University Medical Center, Nashville, TN, USA

Keywords
Endothelial dysfunction · Endothelial nitric oxide synthase · Marfan syndrome · Thoracic aortic aneurysm and dissection · Vasomotor function

Abstract
Introduction: The pathogenic role of nitric oxide (NO) signaling during development of thoracic aortic aneurysm (TAA) in Marfan syndrome (MFS) is currently unclear. We characterized vasomotor function and its relationship to the activity of the NO-generating enzymes in mice with early onset progressively severe MFS. ***Methods:*** Wire myography, immunoblotting, measurements of aortic NO, and superoxide levels were used to compare vasomotor function, contractile protein levels, and the activity of endothelial and inducible NO synthase (eNOS and iNOS, respectively) in ascending thoracic aortas of *Fbn1*$^{mgR/mgR}$ mice relative to wild-type littermates. ***Results:*** Isometric force measurements of aortic rings from 16-day-old male *Fbn1*$^{mgR/mgR}$ mice revealed a significant reduction in acetylcholine-induced relaxation and increased phenylephrine (PE)-promoted contractility, associated with abnormally low eNOS^{Ser1177} phosphorylation, decreased NO production, and augmented superoxide levels. Greater aortic contractility was associated with α1-adrenoceptor upregulation and normal levels of contractile proteins. While iNOS inhibition had no effect on vasomotor functions, mutant aortic rings preincubated with a nonspecific NOS inhibitor yielded a greater PE response, implying a significant contribution of endothelial dysfunction to aortic hypercontractility. ***Conclusion:*** Impaired eNOS signaling disrupts aortic cholinergic relaxation and adrenergic contraction in MFS mice with dissecting TAA.

Plain Language Summary
A thoracic aortic aneurysm is a bulge or weakening in the main artery of the chest, which can be life-threatening if it ruptures. Nitric oxide (NO) is a small gaseous compound produced in the lining of our blood vessels (directly exposed to the bloodstream), which plays a crucial role in keeping our

Keiichi Asano: current address: Life Science Center for Survival Dynamics, Tsukuba Advanced Research Alliance (TARA), University of Tsukuba, Ibaraki 305-8577, Japan

karger@karger.com
www.karger.com/jvr

Correspondence to:
Anna Cantalupo, anna.cantalupo@mssm.edu

blood vessels relaxed and open, ensuring proper flow throughout the body. When the production of NO is impaired, our blood vessels can become less flexible and may not dilate properly, leading to cardiovascular diseases. In our study, we looked at how NO affects the development of thoracic aortic aneurysm in people with Marfan syndrome (MFS), who develop a severe form of aneurysm that can result in its rupture and the death of patients. We used mice that have a severe form of MFS to see how their blood vessels responded compared to normal healthy mice. We found that MFS mice had difficulty relaxing their blood vessels, crucial for proper blood flow, and their vessels were producing excessive force when stimulated with substances that trigger vasoconstriction. This was due to low levels of NO and increased levels of a harmful molecule called superoxide in the MFS mice. Our findings shed light on how NO imbalance contributes to thoracic aortic aneurysm in MFS, which could lead to new treatment options in the future.

Introduction

Marfan syndrome (MFS) is a relatively common connective tissue disorder caused by mutations in fibrillin-1, a large extracellular matrix (ECM) glycoprotein and a major structural component of microfibril fiber networks [1]. Among other manifestations, MFS patients suffer from thoracic aortic aneurysm (TAA) that, left untreated, can lead to an untimely death from acute aortic dissection or rupture [2]. Microfibril fiber networks play a key structural role in supporting aortic homeostasis, as components of the intimal ECM underneath endothelial cells (ECs) and as the concentric elastic lamellae interposed between smooth muscle cell (SMC) layers that constitute the "contractile-elastic unit" [3]. While progressive reduction of the elastic lamella integrity is the structural deficit leading to transmural failure of the MFS aorta, evidence from studies of MFS patients and MFS mice has also implicated endothelial dysfunction in TAA development [4, 5].

The ECs lining the vessel lumen modulate vascular tone and homeostasis through the balanced release of paracrine signals, such as nitric oxide (NO) and endothelin-1, which stimulate vascular SMCs to relax or contract [6]. Intimal EC maintains a basal production of NO from L-arginine by the action of endothelial nitric oxide synthase (eNOS) [7]. Fluid shear stress and various agonists regulate enzyme activity through several different mechanisms, including by modulating eNOS phosphorylation. There is also some evidence of neuronal NOS (nNOS) participation in endothelium-mediated vasorelaxation [8]. In diseased conditions, eNOS uncoupling results in increased production of reactive oxygen species (ROS) at the expense of NO, thus shifting the enzyme role from a vasorelaxant to a prooxidant and inducer of ROS-mediated cellular damage [7]. Additionally, activation of inducible NOS (iNOS) by pro-inflammatory factors leads to chronic release of large quantities of NO that promote superoxide (O_2^-) and peroxynitrite ($ONOO^-$) overproduction [7].

Our current understanding of the molecular determinants of arterial disease in MFS is largely based on experimental evidence gathered from the analysis of two very different mouse models of TAA associated with a fibrillin-1 deficiency. The first mouse model ($Fbn1^{C1041G/+}$) replicates a rarely described form of MFS characterized by late onset of slow developing TAA (up to 12 months) that does not progress to acute aortic dissection and rupture of the vessel wall. The second mouse model ($Fbn1^{mgR/mgR}$) replicates the most commonly diagnosed form of MFS characterized by early onset progressively severe TAA that invariably leads to death from dissection and rupture of the aorta. The substantial differences in arterial disease progression and clinical end points therefore greatly limit our ability to compare data between these 2 mouse models of MFS. Furthermore, and relevant to endothelial dysfunction, distinct abnormalities in NO signaling have been identified by studies of MFS mice with late onset non-dissecting TAA ($Fbn1^{C1041G/+}$ mice). On the one hand, ex vivo myography-based assays correlated impaired endothelial-dependent vasorelaxation with reduced $eNOS^{Ser1177}$ phosphorylation, loss of basal NO production, and augmented ROS levels [5, 9]. On the other hand, pharmacological and genetic experiments associated aneurysm growth and wall degeneration with increased NO bioavailability due to abnormally elevated iNOS activity in the medial layer [10, 11]. Endothelial dysfunction was also reported to have distinct effects on SMC contractility in different mouse models of TAA. Imbalance between enzymes that produce or eliminate O_2^- in the descending thoracic aorta of $Fbn1^{C1041G/+}$ mice was shown to impair SMC contractility [9]. By contrast, ascending thoracic aortas from the same mouse model showed enhanced cyclooxygenase-dependent contractility [12]. Similarly, endothelial dysfunction in mice with postnatal SMC-specific inactivation of the TGFβ receptor 2 ($TBR2^{SM\Delta}$ mice) was associated with aortic hypercontractility due to less NO bioavailability [13].

In this study, we used wire myography and biochemistry to characterize endothelial function and

vasomotor properties of the ascending thoracic aorta of *Fbn1*$^{mgR/mgR}$ mice, a well-characterized preclinical model of dissecting TAA [14]. We chose to focus on postnatal day 16 (P16) to identify early changes in vascular function that may promote disease progression before the onset of aortic dilation [15]. We compare these findings to those observed at P30, when the aorta matures and medial collagen is deposited [16]. The main conclusion of our study is that fibrillin-1 deficiency in the aortic wall impairs eNOS signaling and basal NO production with the result of altering vasomotor function, as evidenced by the inability of mutant aortic rings to properly dilate and contract. We also present evidence suggesting that this abnormality worsens concomitantly to TAA progression.

Materials and Methods

Mice

Fbn1$^{mgR/mgR}$ mice were routinely backcrossed on the C57BL/6J genetic background (Jackson Laboratory, strain 000664) to avoid phenotypic changes due to genetic drift. A total of 312 mice were used to generate all the data presented here: 155 for wire myography and 157 for biochemistry. All experimental mice were males to avoid sex-related variances and, thus, ensure consistency with our previous studies of cardiovascular abnormalities in *Fbn1*$^{mgR/mgR}$ mice [15, 17–20]. Mice were housed on standard laboratory bedding and maintained on a 12-h light-dark cycle. Temperature and humidity were kept within recommended ranges for rodent housing as outlined in institutional animal care guidelines and in accordance with regulatory standards (Institutional Animal Care and Use Committee [IACUC] guidelines; Guide for the Care and Use of Laboratory Animals, 8th edition, National Research Council). The mice were provided ad libitum access to standard laboratory chow (PicoLab Rodent Diet 20; LabDiet.com) and water throughout the study period. All animal procedures were reviewed and approved by the IACUC of the Icahn School of Medicine at Mount Sinai in New York City, ensuring compliance with international standards of Animal Welfare Regulations.

For aortas isolation, *Fbn1*$^{mgR/mgR}$ mice and wild-type (WT) littermates were anesthetized with intraperitoneal injection of ketamine (100 mg/kg) and xylazine (10 mg/kg) and exsanguinated via cold saline perfusion through the left ventricle. Ascending aortic specimens were harvested under a dissecting microscope, spanning from immediately above the aortic root to immediately before the brachiocephalic artery.

Material

All material and reagents used in our study are listed in Table 1.

Wire Myography

Ascending thoracic aorta segment arteries were isolated from P16 and P30 euthanized control and experimental mice and cleaned of surrounding connective tissue. Rings between 1.0 mm and 2.0 mm in length (online suppl. Fig. 1; for all online suppl. material, see https://doi.org/10.1159/000542481) were mounted on a multichamber myograph system (Model 620M, Danish Myo Technology). Two stainless-steel wires (40-μm diameter) were introduced into the lumen of the aortic rings and then fixed to the mounting devices of a force transducer and a micrometer. Viability of the vessels was maintained using Krebs solution (in mM: NaCl 118, KCl 4.7, $MgCl_2$ 1.2, KH_2PO_4 1.2, $CaCl_2$ 2.5, $NaHCO_3$ 25, and glucose 10.1), at 37°C, and gassed with 95% O_2 and 5% CO_2. Aortic rings were stretched until reached a resting tension of 1.5 g, which was determined by preliminary studies by subjecting the tissue to different resting tensions and stimulating with phenylephrine (PE), 1×10^{-9}–3×10^{-5} M and 60 mM KCl buffer [5, 9, 12, 13, 21, 22]. Optimal tension was the same in WT and MFS.

Aortic rings were allowed to stabilize for 30 min and were afterward challenged twice with 60 mM KCl, and then constricted with PE (1 μM) until the responses were reproducible to confirm viability and provide standardization of the rings [5, 9, 12, 13, 21–23]. Constriction was measured by cumulative addition of PE (1×10^{-9}–3×10^{-5} M) and thromboxane analog, U46619 (1×10^{-10}–3×10^{-5} M) on aortic rings at their resting tone. Endothelium-dependent vasorelaxation to acetylcholine (ACh) (1×10^{-9}–3×10^{-5} M) and endothelium-independent vasorelaxation to sodium nitroprusside (1×10^{-10}–3×10^{-7} M) were measured in aortic rings pre-constricted with submaximal dose of PE. In another set of experiments, aortic rings were preincubated with non-selective NOS inhibitor, N(ω)-nitro-L-arginine methyl ester (L-NAME 100 μM for 20 min, Sigma), iNOS inhibitor, 1400W (10 μM for 30 min, Cayman), nNOS inhibitor, N(ω)-propyl-L-arginine (1 μM for 30 min, Sigma), angiotensin II type receptor (AT1R) inhibitor, EXP-3174 (15 μM for 30 min; Cayman), or superoxide dismutase and catalase (150 U/mL and 200 U/mL for 30 min; Sigma). Contractility was normalized over aortic ring wet weight. Data were recorded by using LabChart 8 Pro (ADInstruments).

Table 1. Antibodies and reagents used in the study

Epitope	Origin	Conjugation	Source	Catalog #	Concentration	RRID
Antibodies						
eNOS	Mouse	N/A	BD Biosciences	610296	1/2,000	AB_397690
p-eNOS^{S1177}	Rabbit	N/A	Abcam	ab215717	1/1,000	AB_2893314
iNOS	Rabbit	N/A	Abcam	ab15323	1/500	AB_301857
MYH11	Rabbit	N/A	Abcam	ab124679	1/8,000	AB_10975311
ACTA2	Mouse	N/A	R&D	RB01	1/60,000	
MLC	Rabbit	N/A	Cell Signaling	3672	1/3,000	AB_10692513
p-MLC^{S19}	Rabbit	N/A	Cell Signaling	3671	1/1,000	AB_330248
α1-AR	Mouse	N/A	SCBT	sc-100291	1/2,000	AB_1118870
$TBXA_2R$	Rabbit	N/A	Thermo Scientific	PA5-67751	1/1,000	AB_2691697
GAPDH	Mouse	N/A	Cell Signaling	97166	1/10,000	AB_2756824
Rabbit IgG	Goat	HRP	Cell Signaling	7074S	1/10,000	AB_2099233
Mouse IgG	Horse	HRP	Cell Signaling	7076S	1/10,000	AB_330924

Name	Source	Catalog
Other reagents		
Stain-free labeling protein	Invitrogen	A44449
ACh chloride	Sigma	A6625
PE hydrochloride	Sigma	P6126
SNP dihydrate	Sigma	71778
Iron (II) sulfate heptahydrate	Sigma	12354
Sodium diethyldithiocarbamate trihydrate	Sigma	D3506
DHE	Cayman Chemical	12013
Calcium chloride	Sigma	C4901
Sodium chloride	Sigma	S9888
Potassium chloride	Sigma	P3911
Magnesium sulfate heptahydrate	Sigma	M2773
Potassium phosphate monobasic	Sigma	P0662
Sodium bicarbonate	Sigma	S6014
D-glucose	Sigma	G5767
Trizma hydrochloride	Sigma	T3253
EDTA disodium salt dihydrate	Millipore	324503
L-NAME	Sigma	N5751
1400W	Sigma	W4262
NPA	Sigma	SML2341
EXP-3174	Cayman	15957
SOD	Sigma	S5395
Catalase	Sigma	C1345

SNP, sodium nitroprusside; NPA, N(ω)-propyl-l-arginine; SOD, superoxide dismutase; DHE, dihydroethidium; MLC, myosin light chain.

Electron Spin Resonance

Due to technical limitations, only larger samples of P30 WT and *Fbn1*$^{mgR/mgR}$ mice were used for electron spin resonance (ESR) assay. Briefly, mice were anesthetized with intraperitoneal injection of ketamine (100 mg/kg) and xylazine (10 mg/kg) and quickly perfused via the left ventricle with Krebs-HEPES buffer (in mM: 99.01 NaCl, 4.69 KCl, 2.5 $CaCl_2$, 1.2 $MgSO_4$, 25 $NaHCO_3$, 1.03 K_2HPO_4, 20 Na-HEPES, 5.6 D-glucose, pH 7.35) freshly prepared the day of experiment. For NO assay, thoracic aorta was cleaned of periaortic fat and divided into 5 segments approximately 2.0 mm in length that were placed together in a single well of an ice-cooled 24-well plate, containing 1 mL cold Krebs-HEPES buffer. The segments were then treated with the calcium ionophore A23187 (final concentration 1×10^{-6} M; Enzo Life Sciences) for 15 min at 37°C. During this treatment, a colloidal $Fe(DETC)_2$ solution was prepared by combining equal volumes of 3.2×10^{-5} M of sodium diethyldithiocarbamate (Sigma-Aldrich) and 1.9×10^{-5} M of ferrous sulfate (Sigma-Aldrich), each dissolved separately in 0.9% deoxygenated cold saline. The freshly prepared $Fe(DETC)_2$ solution was immediately added to each well, in dropwise fashion. The segments were incubated at 37°C for 60 min, snap-frozen in fresh Krebs-HEPES buffer in a precut 1 mL syringe, and then stored at −80°C. Samples were removed from syringes as described [24] and placed in a quartz Dewar (Corning, NY) filled with liquid nitrogen. ESR spectra were recorded using an EMX electron spin resonance spectrometer (Bruker BioSpin Corp., Billerica, MA) and a super-high Q microwave cavity [24].

O_2^- Measurements

For O_2^- measurements, ascending thoracic aortas were collected from P30 WT and *Fbn1*$^{mgR/mgR}$ mice ($n = 27$ per genotype), cleaned of periaortic fat, and cut into 2.0-mm-long segments. These aortic segments were pooled together in groups of 3, and each of the resulting 9 experimental and 9 control samples was added to 1 mL of chilled Krebs-HEPES buffer containing the O_2^- probe dihydroethidium (Cayman Chemical) at a final concentration of 50 μM and incubated for 30 min at 37°C in the dark. At the end of the incubation, aortic segments were placed in a single light-insulated tube containing 350 μL of dry-ice-cooled methanol and stored at −80°C for later use. Aortic segments were homogenized with a glass pestle in 350 μL of methanol; the homogenate was passed through a 0.22-μm syringe filter, and the methanol filtrates were analyzed by HPLC according to a previously published protocol[14]. Dihydroethidium oxidation products (2-hydroxyethidium and ethidium) were separated using a C-18 reverse-phase column (Nucleosil 250 to 4.5 mm) and a mobile phase containing 0.1% trifluoroacetic acid and an acetonitrile gradient (from 37% to 47%) at a flow rate of 0.5 mL/min. Ethidium and 2-hydroxyethidium were detected with a fluorescence detector using an emission wavelength of 580 nm and an excitation of 480 nm. Production of cellular O_2^- was measured as accumulation of 2-hydroxyethidium and normalized by protein concentration [24].

Immunoblots

Ascending thoracic aortas spanning from immediately above the aortic root to just before the brachiocephalic artery were quickly harvested from P16 WT and *Fbn1*$^{mgR/mgR}$ mice, cleaned, and snap-frozen in liquid nitrogen. Proteins were extracted by grounding the samples with mortar and pestle and resuspended in 70 μL of Cell Lysis Buffer (Cell Signaling) with addition of protease and phosphatase inhibitor (Sigma). For each Western blot, 10 μg of protein was loaded from each sample, separated on SDS 4–20% gradient gel electrophoresis, and transferred to a PVDF membrane, subsequently probed with antibodies against iNOS (Abcam), myosin heavy chain (MYH11; Abcam), smooth muscle alpha actin (ACTA2; R&D), myosin light chain (MLC; Cell Signaling Technologies), phosphorylated myosin light chain (pMLC; Cell Signaling Technologies), α1 adrenergic receptor (α1-AR; SCBT), and thromboxane A2 receptor ($TBXA_2R$; Thermo Scientific). Bound antibodies were detected with secondary anti-rabbit IgG conjugated to horseradish peroxidase (HRP); sole exceptions were ACTA2 and α1-AR, which were detected with HRP-conjugated anti-mouse. To measure protein levels of eNOS and phosphorylated eNOS, an EC-enriched protein lysate (2–3 μg) was prepared by perfusing aortas with Cell Lysis Buffer (Cell Signaling) according to a previously published protocol [25]. Protein lysates were blotted as described above. Membranes were probed with antibodies against eNOS (BD Biosciences) and p-eNOS^{Ser1177} (Abcam). Bound antibodies were detected with HRP-conjugated anti-mouse and anti-rabbit IgG. PVDF-bound proteins were visualized and measured with ECL solution (GE Healthcare). GAPDH (Cell Signaling) and stain-free labeling protein (Invitrogen) were used as a normalizing internal control [26]. ImageJ was used to quantify band densities.

Statistics

All statistical analyses were performed using GraphPad Prism version 10.0.3. The Shapiro-Wilk test was used to assess the normality of data distribution, with a p value >0.05 indicating normal distribution. Parametric tests were subsequently employed to evaluate statistical differences between the analyzed groups, as assumptions of normality were met. Unpaired T test and one-way ANOVA with Tukey's post hoc test were utilized for comparison

Table 2. E_{max} and EC_{50} values in WT and *Fbn1*$^{mgR/mgR}$ (MFS) mice at indicated age

Stimulus	E_{max}	Statistic
ACh	P16 MFS 91.6±1.49 versus P16 WT 97.9±0.52%	*T* test, $p = 0.0016$
ACh	P30 MFS 84.5±3.41 versus P30 WT 99.5±0.31%	*T* test, $p = 0.0006$
ACh	P30 MFS 84.5±3.41 versus P16 MFS 91.6±1.49%	*T* test, $p = 0.0357$
SNP	P16 MFS 99.0±1.60 versus P16 WT 100±0.00%	*T* test, $p = 0.0762$
SNP	P30 MFS 99.7±0.75 versus P30 WT 99.2±0.27%	*T* test, $p = 0.6055$
PE	P16 MFS 0.39±0.04 versus P16 WT 0.24±0.03 g/mg wet tissue	*T* test, $p = 0.0311$
PE	P30 MFS 1.1±0.07 versus P30 WT 0.8±0.04 g/mg wet tissue	*T* test, $p = 0.0023$
U46619	P16 MFS 0.77±0.23 versus P16 WT 0.73±0.24 g/mg wet tissue	*T* test, $p = 0.8076$
KCl (60 mM)	P16 MFS 0.17±0.02 versus P16 WT 0.21±0.03 g/mg wet tissue	*T* test, $p = 0.2264$
PE	P16 MFS 292.4±28.07 versus P16 WT 178.4±31.05%	*T* test, $p = 0.0139$
Stimulus	EC_{50}	Statistic
ACh	P16 MFS −6.9±0.08 versus P16 WT −7.4±0.06 logM	*T* test, $p < 0.0001$
ACh	P30 MFS −6.7±0.21 versus P30 WT −7.6±0.27 logM	*T* test, $p < 0.0001$
ACh	P30 MFS −6.7±0.21 versus P16 MFS −6.9±0.37 logM	*T* test, $p = 0.0954$
SNP	P16 MFS −8.4±0.31 versus P16 WT −8.9±0.28 logM	*T* test, $p = 0.0066$
SNP	P30 MFS −8.2±0.14 versus P30 WT 8.4±0.11 logM	*T* test, $p = 0.3264$
PE	P16 MFS −6.7±0.37 versus P16 WT −6.5±0.26 logM	*T* test, $p = 0.0843$
U46619	P16 MFS −8.306±0.2687 versus P16 WT −8.064±0.2756 logM	*T* test, $p = 0.1772$

SNP, sodium nitroprusside.

between two groups, while two-way ANOVA followed by Tukey's multiple comparisons post hoc test was applied for the myography results. $p < 0.05$ was considered statistically significant. Statistically significant differences were denoted by asterisks signifying $*p \leq 0.05$, $**p \leq 0.01$, $***p \leq 0.001$, $****p \leq 0.0001$. Data are presented as mean ± SEM.

Results

TAA Is Associated with Impaired Endothelium-Dependent Relaxation

Wire myography was used to characterize the vasomotor properties of the ascending thoracic aorta of *Fbn1*$^{mgR/mgR}$ mice. These mutant mice are homozygous for a hypomorphic *Fbn1* mutation, invariably die from TAA dissection, and rupture within the first 5–6 months of postnatal life (median survival ~3 months of age) [14, 17]. Several in vivo studies have demonstrated that abnormally high signaling by the AT1R, a stimulator of SMC contractility, is a major contributor to TAA progression in MFS mice [1].

To evaluate endothelium-dependent vasorelaxation, ACh was cumulatively added to 16-day-old (P16) mutant and WT aortic rings pre-constricted with PE. This approach revealed a significantly reduced relaxation (Table 2, E_{max}: mutant 91.6 ± 1.49% vs. WT 97.9 ± 0.52%) and sensitivity to ACh of mutant relative to WT samples (Table 2, EC_{50}: mutant −6.9 ± 0.08 logM vs. WT −7.4 ± 0.06 logM; Fig. 1a). By contrast, maximal relaxation was unremarkable when the exogenous NO donor sodium nitroprusside was added to the bathing solution of mutant aortic rings (Table 2, E_{max}: P16 mutant 99 ± 1.6% vs. WT 100 ± 0.00%). However, sensitivity was only mildly and transiently altered (Fig. 1b and Table 2), with mutant segments isolated at P30 showing no significant difference from their WT counterparts (online suppl. Fig. 2A). Therefore, our data excluded a major functional defect of SMC. Of note, maximal relaxation was markedly more reduced in aortic rings from P30 *Fbn1*$^{mgR/mgR}$ mice than those isolated at P16 (Table 2, E_{max}: P30 84.5 ± 3.41 vs. P16 91.6 ± 1.49%; Fig. 1a, and ACh concentration-response curve at P30 in online suppl. Fig. 2B).

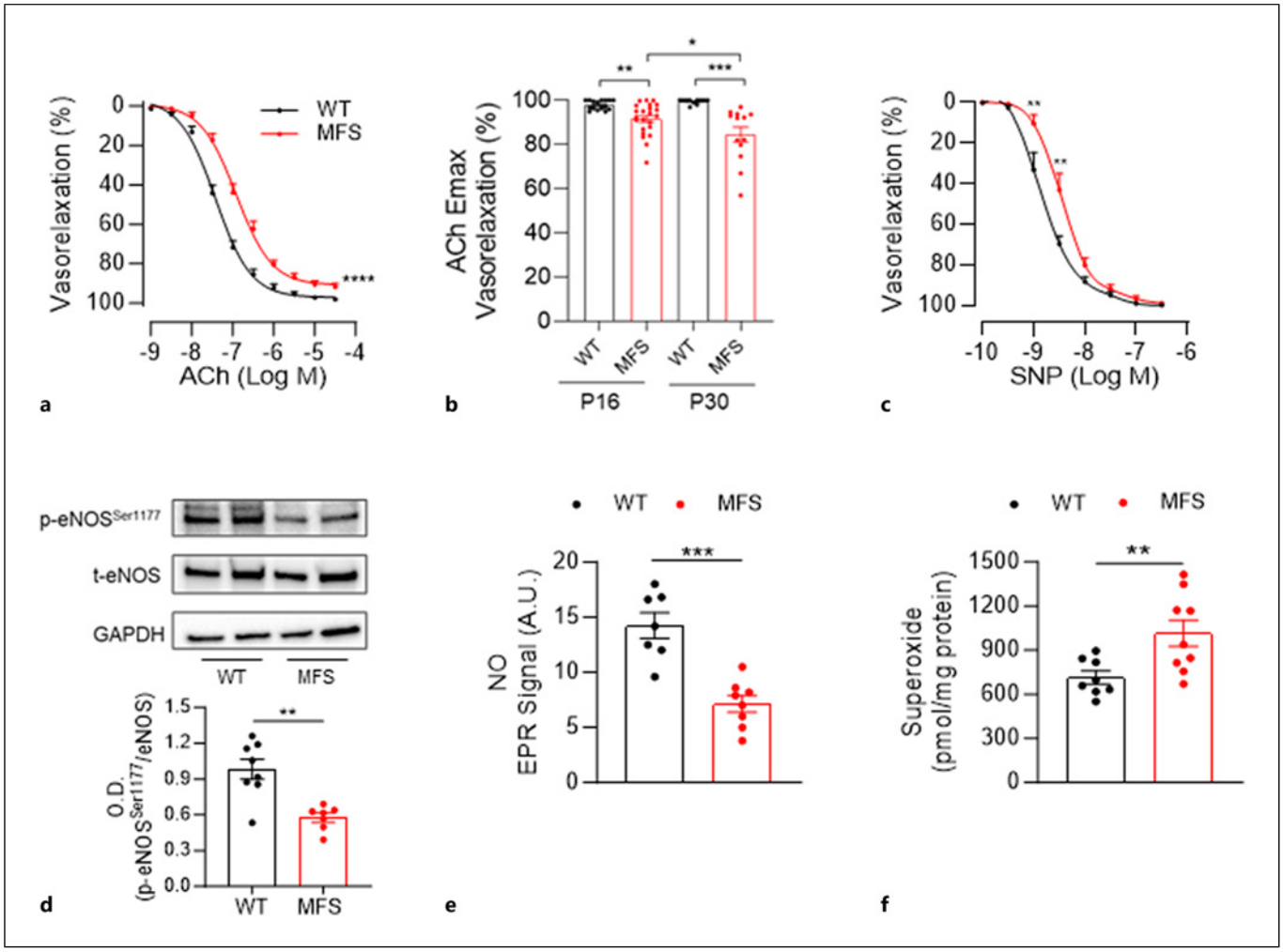

Fig. 1. a Endothelium-dependent vasorelaxation assessed via cumulative dose-response curves to ACh of PE pre-constricted aortic rings isolated from P16 *Fbn1*$^{mgR/mgR}$ mice (MFS; $n = 23$) and WT ($n = 16$) littermates. **b** Extrapolation of ACh-induced relaxation maximal effect (E_{max}) in P16 and P30 WT ($n = 11$) and MFS ($n = 13$) mice. **c** Endothelium-independent vasorelaxation assessed via cumulative dose-response curves to SNP of PE pre-constricted aortic rings isolated from P16 *Fbn1*$^{mgR/mgR}$ mice (MFS; $n = 11$) and WT ($n = 9$) littermates. **d** Representative immunoblots of p-eNOS^{Ser1177} and t-eNOS in endothelium-enriched protein extracts from the ascending aortas of P16 WT and *Fbn1*$^{mgR/mgR}$ (MFS) mice with quantitative plots shown below represented as p-eNOS^{Ser1177}/eNOS ratio determined by densitometric analysis. GAPDH was used as a loading control. **e** Levels of endothelial-derived NO measured in the ascending aorta of P30 WT and *Fbn1*$^{mgR/mgR}$ (MFS) mice with EPR spectroscopy. **f** O_2^- levels in aortic rings isolated from P30 WT and *Fbn1*$^{mgR/mgR}$ (MFS) measured by DHE method. Asterisks indicate statistical significance. SNP, sodium nitroprusside; DHE, dihydroethidium; EPR, electron paramagnetic resonance; t-eNOS, total eNOS.

Endothelial Dysfunction Is Associated with Compromised eNOS Signaling

Based on the above findings, we assessed eNOS phosphorylation at Ser^{1177}, a critical requirement for the enzyme catalytic activity[7]. To this end, ascending thoracic aortas of *Fbn1*$^{mgR/mgR}$ mice and WT littermates were perfused with a protein extraction buffer to chemically strip-off the endothelium. Immunoblotting experiments detected significantly less p-eNOS^{Ser1177} in EC-enriched perfusates from mutant than WT aortas (Fig. 1c). Consistent with this finding, detection of eNOS-produced NO using electron paramagnetic resonance with ferrous dithiocarbamate for NO spin trap revealed ~50% less NO in mutant compared to WT aortas (Fig. 1d). Additional ex vivo analyses showed higher than normal levels of O_2^- in the aorta of *Fbn1*$^{mgR/mgR}$ mice (Fig. 1e).

It was recently reported that iNOS stimulation in the tunica media is the major driver of aneurysm growth and

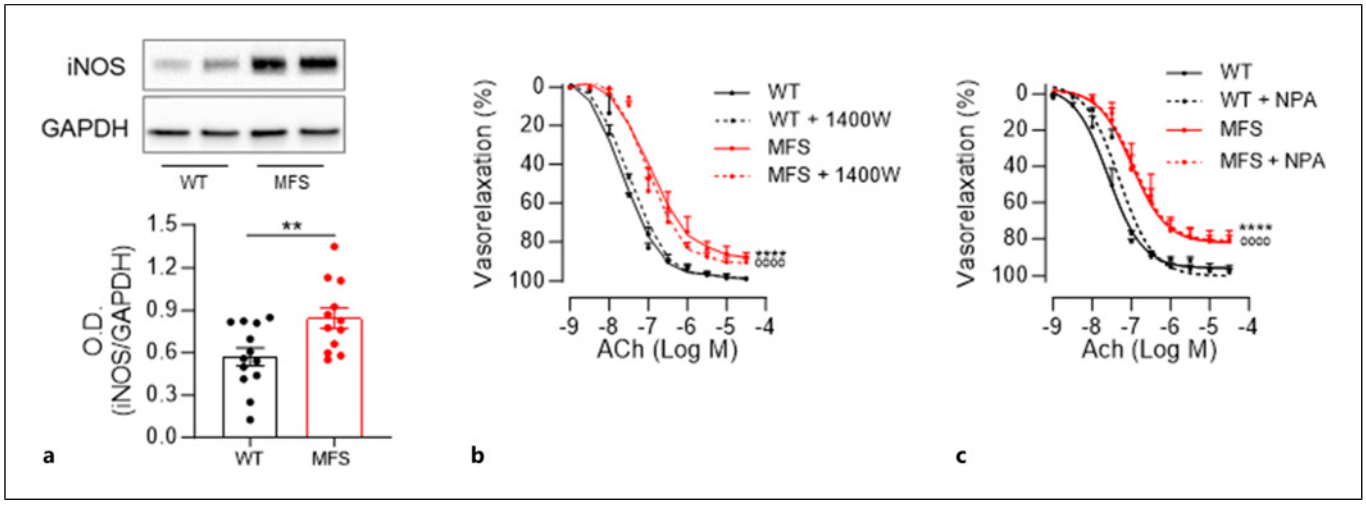

Fig. 2. a Representative iNOS immunoblots in protein extracts from the ascending aortas of P16 WT and *Fbn1*$^{mgR/mgR}$ (MFS) mice with quantitative plots shown on the bottom. GAPDH was used as a loading control. **b** ACh-dependent vasorelaxation assessed in aortic ring isolated from *Fbn1*$^{mgR/mgR}$ mice (MFS) and WT littermates before and after incubation with iNOS inhibitor, 1400W (n = 3 per genotype and treatment). **c** ACh-dependent vasorelaxation assessed in aortic ring isolated from *Fbn1*$^{mgR/mgR}$ mice (MFS) and WT littermates before and after incubation with nNOS inhibitor, NPA (n = 4 per genotype and treatment). Asterisks indicate statistical significance. NPA, N(ω)-propyl-L-arginine.

wall degeneration in *Fbn1*$^{C1041G/+}$ mice, a preclinical animal model of non-dissecting TAA [10, 11]. Immunoblotting experiments documented a similar abnormal increase of iNOS levels in the ascending thoracic aorta of P16 *Fbn1*$^{mgR/mgR}$ mice (Fig. 2a). Next, we tested whether overproduction of iNOS-generated NO in the medial layer of the fibrillin-1 deficient aorta may contribute to endothelial dysfunction. Wire myography assays ruled out this possibility by showing similar ACh responses by mutant and WT aortic rings preincubated with the iNOS inhibitor, 1400W (Fig. 2b). No changes in ACh-induced relaxation were also observed when aortic rings from *Fbn1*$^{mgR/mgR}$ mice were preincubated with the nNOS inhibitor, N(ω)-propyl-L-arginine (Fig. 2c). We therefore concluded that eNOS dysfunction is the main cause of impaired vasorelaxation.

Fibrillin-1 Deficiency Causes Aortic Hypercontractility

The next set of wire myography assays compared contractility of mutant and WT ascending thoracic aortas. *Fbn1*$^{mgR/mgR}$ aortic rings developed higher force in response to PE, an α1-AR agonist (Table 2, E_{max}: mutant 0.39 ± 0.04 vs. WT 0.24 ± 0.03 g/mg wet tissue; EC_{50}: mutant −6.7 ± 0.37 logM vs. WT −6.5 ± 0.26 logM), but not to KCl, a trigger of receptor-independent vasoconstriction (Table 2, mutant 0.17 ± 0.02 vs. WT 0.21 ± 0.03 g/mg wet tissue) (Fig. 3a, b). When PE-induced constriction was normalized to KCl-induced contractile force, the difference between mutant and WT aortas was still significant (Table 2, E_{max}: mutant 292.4 ± 28.07% vs. WT 178.4 ± 31.05%), indicating receptor-dependent hypercontractility (Fig. 3c). By contrast, no differences were observed between *Fbn1*$^{mgR/mgR}$ and WT aortic rings when contractile forces were measured in response to U46619, a stable mimetic of thromboxane A2 (Fig. 3d). Like TBR2$^{SM\Delta}$ mice [13], immunoblotting experiments revealed that hypercontractility was associated with no significant differences in the levels of major SMC contractile proteins MYH11, ACTA2, MLC, and p-MLC^{Ser19} (online suppl. Fig. 3). However, a substantial increase in α1-AR expression (Fig. 3e) and normal $TBXA_2R$ levels in *Fbn1*$^{mgR/mgR}$ samples (Fig. 3f) were detected consistently with PE-induced hypercontractility. Like impaired relaxation, aortic hypercontractility was more severe at P30 than P16 (Table 2, E_{max}: mutant 1.1 ± 0.07 vs. WT 0.8 ± 0.04 g/mg wet tissue) (online suppl. Fig. 4).

Endothelial Dysfunction Contributes to Aortic Hypercontractility

To identify potential contributors to aortic hypercontractility, PE concentration-response curves were evaluated in mutant and WT aortic rings preincubated with inhibitors of NOS, ROS, and AT1R signaling. Preincubation with nonspecific NOS inhibitor, L-NAME, resulted in increased sensitivity to PE of mutant relative to WT aortic rings (EC_{50} mutant −9.2 ± 0.43 logM vs.

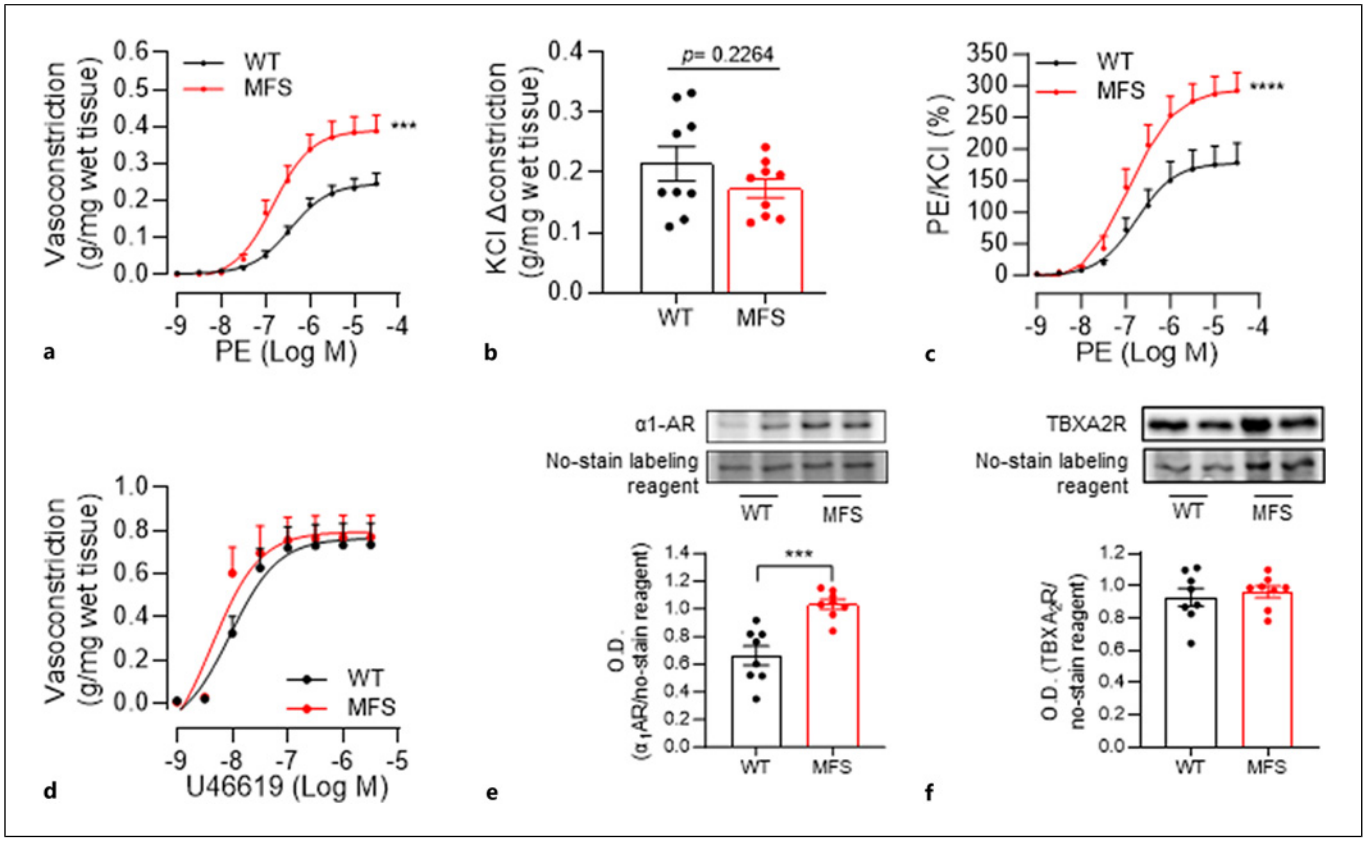

Fig. 3. a Cumulative concentration-response curve to PE in aortic rings isolated from P16 *Fbn1*$^{mgR/mgR}$ mice (MFS; n = 12) and WT (n = 7). **b** KCl-induced vasoconstriction in aortic ring isolated from *Fbn1*$^{mgR/mgR}$ mice (MFS; n = 9) and WT littermates (n = 9). **c** PE-induced vasoconstriction normalized over KCl maximal vasoconstriction. **d** Cumulative concentration-response curve to U46619, a $TBXA_2$ mimetic, in aortic rings isolated from *Fbn1*$^{mgR/mgR}$ mice (MFS; n = 5) and WT littermates (n = 6). Representative α1-AR (**e**) and $TBXA_2R$ (**f**) immunoblots of protein extracts from ascending thoracic aortas of WT and *Fbn1*$^{mgR/mgR}$ (MFS) mice with quantitative plots shown on the bottom. No-stain labeling reagent was used as an internal control. Asterisks indicate statistical significance. $TBXA_2$, thromboxane A2.

WT −7.9 ± 0.18 logM), thus confirming α1-AR upregulation in the former samples (Fig. 4a). The fact that the area under the curve is greater in MFS compared to WT group after L-NAME treatment (Fig. 4b) indicates that other vasoconstrictor pathways, other than NO, may be involved. This is consistent with the interpretation that NO normally plays a role in modulating vascular tone, and its absence in part contributes to increased vascular contractility. Consistent with this conclusion, preincubation with the iNOS-specific inhibitor 1400W had virtually no effect on PE-induced force contractility of *Fbn1*$^{mgR/mgR}$ aortic rings (Fig. 4c). Similar negative results were obtained when the response to PE stimulation was evaluated after preincubating the aortic rings with either a combination of superoxide dismutase and catalase to inhibit ROS action, or the active losartan metabolite EXP-3174 to inhibit excessive AT1R signaling (Fig. 4d, e). Altogether, our findings indicate that endothelium-dependent vasomotor dysfunction contributes to the progression of dissecting TAA in MFS.

Discussion

Endothelial dysfunction associated with impaired NO signaling is implicated in the pathophysiology of several cardiovascular diseases, including TAA in MFS [1]. The earliest evidence of endothelial dysfunction in MFS was provided by a small clinical study that found abnormally low vasodilatory response to blood flow and ACh-mediated stimulation of NO-dependent relaxation of the brachial artery [4]. Subsequent ex vivo analyses of *Fbn1*$^{C1041G/+}$ mice supported these human findings by showing impaired endothelial function and eNOS-mediated NO production in

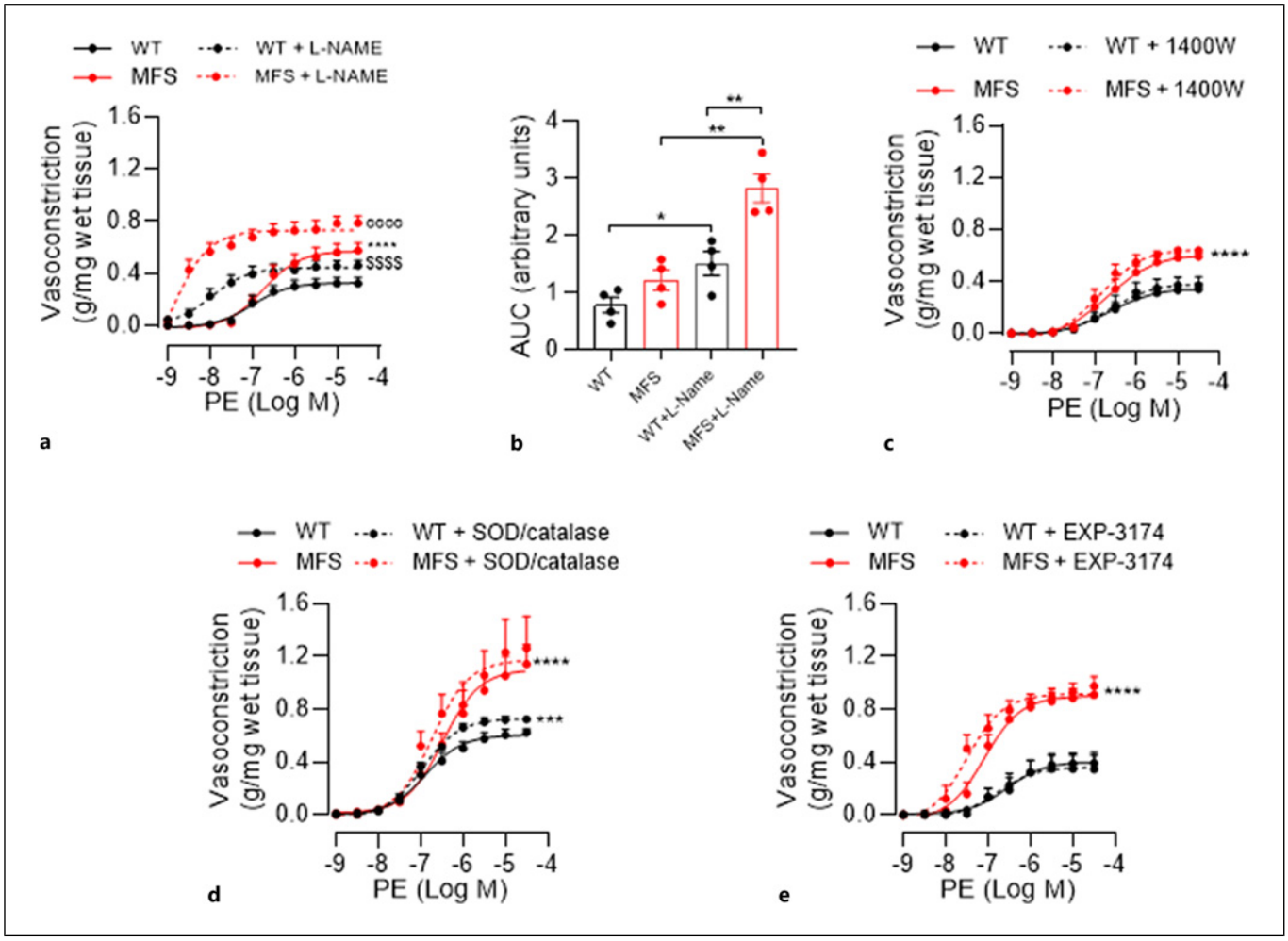

Fig. 4. PE-dependent vasoconstriction (**a**) and analysis of AUC (**b**) in the presence or absence of the non-selective NOS inhibitor, L-NAME, in aortic ring isolated from P16 *Fbn1*$^{mgR/mgR}$ mice (MFS) and WT littermates (n = 4 per genotype and treatment). **c** PE-dependent vasoconstriction assessed in aortic ring isolated from P16 *Fbn1*$^{mgR/mgR}$ mice (MFS) and WT littermates before and after incubation with iNOS inhibitor, 1,400W (n = 3 per genotype and treatment). **d** PE-dependent vasoconstriction assessed in aortic ring isolated from P16 *Fbn1*$^{mgR/mgR}$ mice (MFS; n = 5 per treatment) and WT littermates (n = 3 per treatment) before and after incubation with SOD+catalase inhibitor. **e** PE-dependent vasoconstriction assessed in aortic ring isolated from P16 *Fbn1*$^{mgR/mgR}$ mice (MFS; n = 4) and WT littermates (n = 4) before and after incubation with EXP-3174, an active metabolite of AT1R inhibitor, losartan. Asterisks indicate statistical significance. SOD, superoxide dismutase; AUC, area under the curve.

the aorta [5]. However, more recent studies using the same preclinical model of MFS with non-dissecting TAA have implicated overactivation of iNOS signaling in TAA onset [10, 11], suggesting that NO signaling blockade might be an effective treatment strategy [27]. Here, we examined endothelial signaling and vasomotor function in MFS mice with dissecting TAA.

Our experiments indicate that fibrillin-1 deficiency in the ascending thoracic aorta reduces endothelium-dependent relaxation, as a result of impaired eNOS activity as well as NO/O_2^- balance. This vasomotor impairment exacerbates concomitantly to TAA progression. Like the milder *Fbn1*$^{C1041G/+}$ mouse, we also found abnormally high levels of iNOS in the ascending thoracic aorta of our mouse model of early onset progressively severe MFS. Although stimulated iNOS can produce vastly more NO than the constitutively active eNOS and nNOS, no changes were recorded in response to ACh stimulation when *Fbn1*$^{mgR/mgR}$ aortic rings were preincubated with an iNOS inhibitor. Similar negative results were obtained using a nNOS inhibitor as well. We do not dispute the observation that iNOS is overexpressed; however, our findings suggest that this overexpression does

not contribute to vascular function in the Marfan aorta, as evidenced by the lack of significant changes in relaxation responses following preincubation with selective iNOS inhibitor, 1400W. This reinforces our conclusion that impaired eNOS signaling is the primary driver of endothelial dysfunction and compromised vasorelaxation, thereby questioning the prior conclusion that iNOS inhibitors could be a viable strategy to manage dissecting TAA in MFS and potentially in other presentations of arterial disease [11]. It also reemphasizes the previously mentioned limitations of comparing two different mouse models of TAA in terms of both progression rate and end points.

While the levels of proteins implicated in aortic SMC contractility were unchanged, our ex vivo tests revealed an association between fibrillin-1 deficiency and greater than normal contractile response to PE. This finding appears to conflict with the prevailing view that decreased SMC contractile unit function is associated with aneurysm formation. However, it aligns with other studies reporting aortic hypercontractility in models of MFS, including the *Fbn1*$^{C1041G/+}$ mice, while the descending aorta displays hypocontractility [12]. Additionally, a recent study identified aortic hypercontractility in mice with specific loss of Tgfβr2 in SMC, which was associated with endothelial dysfunction resulting from signal relay from SMC to EC [13]. Our data also correlated aortic hypercontractility with significantly higher than normal levels of α1-AR and, in part, with endothelial dysfunction. By performing isometric force measurements in the presence of specific inhibitors, we also ruled out the possibility that elevated ROS or AT1R signaling in the *Fbn1*$^{mgR/mgR}$ aorta might contribute to increased SMC contractility. Although our study primarily focused on the association between fibrillin-1 deficiency and NO dysregulation in relation to SMC contractility, we acknowledge that additional factors, such as alterations in prostanoid signaling, may contribute to the observed phenotype and have been previously reported in non-dissecting *Fbn1*$^{C1041G/+}$ mouse model of MFS [12, 23]. Specifically, dysregulated production or sensitivity to prostanoids could potentially exacerbate vascular dysfunction in *Fbn1*$^{mgR/mgR}$ mice, leading to enhanced vasoconstrictor responses and aberrant vascular remodeling. Of note, one technical limitation of our study is that we measured NO levels with the ESR method in stimulated vessels with the addition of a calcium ionophore rather than at baseline (without stimulus). While this approach may limit our ability to assess NO levels under resting conditions, it still provides valuable insight into endothelial function. However, the ESR method's advantage lies in its ability to selectively measure endothelial-derived NO, thereby avoiding potential bias from other sources such as iNOS. Lastly, our study was conducted exclusively using male mice, consistent with our previous investigations of TAA in MFS [14, 15, 17–20, 28]. However, given recent evidence of TAA sexual dimorphism in MFS mice [12, 29], our findings underscore the importance of comparing endothelial dysfunction in the aorta of female *Fbn1*$^{mgR/mgR}$ mice.

While our study primarily characterizes the functional consequences of fibrillin-1 deficiency in the *Fbn1*$^{mgR/mgR}$ mouse model, we acknowledge the need for deeper exploration of the mechanistic links between fibrillin-1 deficiency and endothelial dysfunction. Fibrillin-1 is essential for maintaining the integrity of microfibril networks within the ECM, and its absence leads to significant mechanical changes in the aortic wall [20, 30]. Given that ECs are highly responsive to mechanical stimuli from the underlying ECM, the disruption of these structural components may contribute to the observed endothelial dysfunction.

To further elucidate these mechanistic pathways, the development of a mouse model with targeted deletion of fibrillin-1 specifically in ECs would be particularly informative. This approach could enable direct assessment of the impact of fibrillin-1 loss on endothelial function and NO signaling, providing crucial insights into the causative relationships at play.

Additionally, the correlation observed between fibrillin-1 deficiency and endothelial dysfunction in both the *Fbn1*$^{mgR/mgR}$ and *Fbn1*$^{C1041G/+}$ models indicates a consistent pattern of impairment associated with this gene mutation. By investigating these links, future studies could enhance our understanding of how fibrillin-1 deficiency contributes to the vascular complications of MFS and inform the development of new effective therapeutic approaches to manage this condition.

Acknowledgments

We thank Dr. D. Rifkin for critical review of the manuscript, B. Crockett for outstanding technical support, and K. Johnson for organizing the manuscript.

Statement of Ethics

This study protocol was reviewed and approved by the Institutional Animal Care and Use Committee of Icahn School of Medicine at Mount Sinai, NY, protocol 08-0276 (Francesco Ramirez, PI).

Conflict of Interest Statement

The authors have no conflicts of interest to declare.

Funding Sources

This work was supported by the National Institutes of Health (NIH) Grants P01HL134605 (to F.R.), and R01HL144943 and R01HL157583 (to S.D.); additional support was by the Marfan Foundation, Early Career Investigator Award (to A.C.), and by the Elster Research Endowment (to F.R.).

Author Contributions

Anna Cantalupo, Asano Keiichi, and Francesco Ramirez contributed to conception and design of the study. Anna Cantalupo and Dylan Gordon completed most of the experimental work. Sergey Dikalov performed NO and O_2^- measurements. Anna Cantalupo and Asano Keiichi completed data analysis. Dylan Gordon had oversight of mouse husbandry and genotyping. Francesco Ramirez provided funding, resources, and oversight of the project. Francesco Ramirez and Anna Cantalupo wrote the first draft of the manuscript. All authors contributed to manuscript revision, and read and approved the submitted version.

Data Availability Statement

All data generated or analyzed during this study are included in this article and in its supplementary material files. Further inquiries can be directed to the corresponding authors.

References

1 Asano K, Cantalupo A, Sedes L, Ramirez F. Pathophysiology and therapeutics of thoracic aortic aneurysm in marfan syndrome. Biomolecules. 2022;12(1):128. https://doi.org/10.3390/biom12010128
2 Milewicz DM, Braverman AC, De Backer J, Morris SA, Boileau C, Maumenee IH, et al. Marfan syndrome. Nat Rev Dis Primers. 2021;7(1):64. https://doi.org/10.1038/s41572-021-00298-7
3 Wagenseil JE, Mecham RP. Vascular extracellular matrix and arterial mechanics. Physiol Rev. 2009;89(3):957–89. https://doi.org/10.1152/physrev.00041.2008
4 Wilson DG, Bellamy MF, Ramsey MW, Goodfellow J, Brownlee M, Davies S, et al. Endothelial function in Marfan syndrome. Selective impairment of flow-mediated vasodilation. Circulation. 1999;99(7):909–15. https://doi.org/10.1161/01.cir.99.7.909
5 Chung AWY, Au Yeung K, Cortes SF, Sandor GGS, Judge DP, Dietz HC, et al. Endothelial dysfunction and compromised eNOS/Akt signaling in the thoracic aorta during the progression of Marfan syndrome. Br J Pharmacol. 2007;150(8):1075–83. https://doi.org/10.1038/sj.bjp.0707181
6 Sandoo A, van Zanten JJCSV, Metsios GS, Carroll D, Kitas GD. The endothelium and its role in regulating vascular tone. Open Cardiovasc Med J. 2010;4:302–12. https://doi.org/10.2174/1874192401004010302
7 Forstermann U, Sessa WC. Nitric oxide synthases: regulation and function. Eur Heart J. 2012;33(7):829–37. https://doi.org/10.1093/eurheartj/ehr304
8 Costa ED, Rezende BA, Cortes SF, Lemos VS. Neuronal nitric oxide synthase in vascular physiology and diseases. Front Physiol. 2016;7:206. https://doi.org/10.3389/fphys.2016.00206
9 Yang HHC, van Breemen C, Chung AWY. Vasomotor dysfunction in the thoracic aorta of Marfan syndrome is associated with accumulation of oxidative stress. Vascul Pharmacol. 2010;52(1–2):37–45. https://doi.org/10.1016/j.vph.2009.10.005
10 Oller JM-BN, Méndez-Barbero N, Ruiz EJ, Villahoz S, Renard M, Canelas LI, et al. Nitric oxide mediates aortic disease in mice deficient in the metalloprotease Adamts1 and in a mouse model of Marfan syndrome. Nat Med. 2017;23(2):200–12. https://doi.org/10.1038/nm.4266
11 De la Fuente-Alonso A, Toral M, Alfayate A, Ruiz-Rodríguez MJ, Bonzon-Kulichenko E, Teixido-Tura G, et al. Aortic disease in Marfan syndrome is caused by overactivation of sGC-PRKG signaling by NO. Nat Commun. 2021;12(1):2628. https://doi.org/10.1038/s41467-021-22933-3
12 Jiménez-Altayó F, Siegert AM, Bonorino F, Meirelles T, Barbera L, Dantas AP, et al. Differences in the thoracic aorta by region and sex in a murine model of marfan syndrome. Front Physiol. 2017;8:933. https://doi.org/10.3389/fphys.2017.00933
13 Zhu J, Angelov S, Alp Yildirim I, Wei H, Hu JH, Majesky MW, et al. Loss of transforming growth factor beta signaling in aortic smooth muscle cells causes endothelial dysfunction and aortic hypercontractility. Arterioscler Thromb Vasc Biol. 2021;41(6):1956–71. https://doi.org/10.1161/ATVBAHA.121.315878
14 Pereira L, Lee SY, Gayraud B, Andrikopoulos K, Shapiro SD, Bunton T, et al. Pathogenetic sequence for aneurysm revealed in mice underexpressing fibrillin-1. Proc Natl Acad Sci U S A. 1999;96(7):3819–23. https://doi.org/10.1073/pnas.96.7.3819
15 Cook JR, Clayton NP, Carta L, Galatioto J, Chiu E, Smaldone S, et al. Dimorphic effects of transforming growth factor-β signaling during aortic aneurysm progression in mice suggest a combinatorial therapy for Marfan syndrome. Arterioscler Thromb Vasc Biol. 2015;35(4):911–7. https://doi.org/10.1161/ATVBAHA.114.305150
16 Murtada S-I, Kawamura Y, Li G, Schwartz MA, Tellides G, Humphrey JD. Developmental origins of mechanical homeostasis in the aorta. Dev Dyn. 2021;250(5):629–39. https://doi.org/10.1002/dvdy.283
17 Cook JR, Carta L, Benard L, Chemaly ER, Chiu E, Rao SK, et al. Abnormal muscle mechanosignaling triggers cardiomyopathy in mice with Marfan syndrome. J Clin Invest. 2014;124(3):1329–39. https://doi.org/10.1172/JCI71059
18 Galatioto J, Caescu CI, Hansen J, Cook J, Miramontes I, Iyengar R, et al. Cell type-specific contributions of the angiotensin II type 1a receptor to aorta homeostasis and aneurysmal disease-brief report. Arterioscler Thromb Vasc Biol. 2018;38(3):588–91. https://doi.org/10.1161/ATVBAHA.117.310609
19 Hansen J, Galatioto J, Caescu CI, Arnaud P, Calizo RC, Spronck B, et al. Systems pharmacology-based integration of human and mouse data for drug repurposing to treat thoracic aneurysms. JCI Insight. 2019;4(11):e127652. https://doi.org/10.1172/jci.insight.127652
20 Caescu CI, Hansen J, Crockett B, Xiao W, Arnaud P, Spronck B, et al. Inhibition of HIPK2 alleviates thoracic aortic disease in mice with progressively severe marfan syndrome. Arterioscler Thromb Vasc Biol. 2021;41(9):2483–93. https://doi.org/10.1161/ATVBAHA.121.316464
21 Gibson C, Nielsen C, Alex R, Cooper K, Farney M, Gaufin D, et al. Mild aerobic exercise blocks elastin fiber fragmentation and aortic dilatation in a mouse model of Marfan syndrome associated aortic aneurysm. J Appl Physiol. 2017;123(1):147–60. https://doi.org/10.1152/japplphysiol.00132.2017
22 Bucci M, Papapetropoulos A, Vellecco V, Zhou Z, Zaid A, Giannogonas P, et al. cGMP-dependent protein kinase contributes to hydrogen sulfide-stimulated vasorelaxation. PLoS One. 2012;7(12):253319. https://doi.org/10.1371/journal.pone.0053319

23 Chung AWY, Yang HHC, van Breemen C. Imbalanced synthesis of cyclooxygenase-derived thromboxane A2 and prostacyclin compromises vasomotor function of the thoracic aorta in Marfan syndrome. Br J Pharmacol. 2007;152(3):305–12. https://doi.org/10.1038/sj.bjp.0707391
24 Dikalova AE, Bikineyeva AT, Budzyn K, Nazarewicz RR, McCann L, Lewis W, et al. Therapeutic targeting of mitochondrial superoxide in hypertension. Circ Res. 2010;107(1):106–16. https://doi.org/10.1161/CIRCRESAHA.109.214601
25 McDonald AI, Shirali AS, Aragon R, Ma F, Hernandez G, Vaughn DA, et al. Endothelial regeneration of large vessels is a biphasic process driven by local cells with distinct proliferative capacities. Cell Stem Cell. 2018;23(2):210–25.e6. https://doi.org/10.1016/j.stem.2018.07.011
26 Diller T, Thompson J, Steer B. Biological validation of a novel process and product for quantitating western blots. J Biotechnol. 2021;326:52–60. https://doi.org/10.1016/j.jbiotec.2020.12.012
27 Toral M, de la Fuente-Alonso A, Campanero MR, Redondo JM. The NO signaling pathway in aortic aneurysm and dissection. Br J Pharmacol. 2022;179:1287–303.
28 Sun Y, Asano K, Sedes L, Cantalupo A, Hansen J, Iyengar R, et al. Dissecting aortic aneurysm in Marfan syndrome is associated with losartan-sensitive transcriptomic modulation of aortic cells. JCI Insight. 2023;8(10):e168793. https://doi.org/10.1172/jci.insight.168793
29 Budbazar E, Sulser Ponce De Leon S, Tsukahara Y, Liu H, Huangfu Y, Wang Y, et al. Redox Dysregulation of Vascular smooth muscle sirtuin-1 in thoracic aortic aneurysm in Marfan syndrome. Arterioscler Thromb Vasc Biol. 2023;43(8):e339–57. https://doi.org/10.1161/ATVBAHA.123.319145
30 Cavinato C, Chen M, Weiss D, Ruiz-Rodriguez MJ, Schwartz MA, Humphrey JD. Progressive microstructural deterioration dictates evolving biomechanical dysfucntion in the Marfan aorta. Front Cardiovasc Med. 2021;8:800730. https://doi.org/10.3389/fcvm.2021.800730